

# Optical Engineering

OpticalEngineering.SPIEDigitalLibrary.org

## **Tungsten oxide–cellulose nanocrystal composite films for electrochromic applications**

Stefan Stoenescu  
Simona Badilescu  
Tanu Sharma  
Ralf Brüning  
Vo-Van Truong

**SPIE.**

Stefan Stoenescu, Simona Badilescu, Tanu Sharma, Ralf Brüning, Vo-Van Truong, “Tungsten oxide–cellulose nanocrystal composite films for electrochromic applications,” *Opt. Eng.* **55**(12), 127102 (2016), doi: 10.1117/1.OE.55.12.127102.

# Tungsten oxide–cellulose nanocrystal composite films for electrochromic applications

Stefan Stoenescu,<sup>a</sup> Simona Badilescu,<sup>a</sup> Tanu Sharma,<sup>b</sup> Ralf Brüning,<sup>b</sup> and Vo-Van Truong<sup>a,\*</sup>

<sup>a</sup>Concordia University, Department of Physics, 7141 Sherbrooke Street West, Montréal, Quebec, H4B 1R6, Canada

<sup>b</sup>Mount Allison University, Department of Physics, 67 York Street, Sackville, New Brunswick, E4L 1E6, Canada

**Abstract.** Composite films of tungsten oxide and CNCs are prepared through a sol–gel method and their electrochromic (EC) properties investigated. After mixing CNC gel into a tungsten oxide precursor solution, indium-tin-oxide-coated glass substrates are dipped into the composite solution and subsequently annealed at 170°C. The composite films consisted of CNCs dispersed in the tungsten oxide matrix. The resulting nanocomposite was found to be amorphous, exhibiting a high transmission modulation and very good cycling stability. After having tested a range of compositions, a film of WO<sub>3</sub> with 10% CNC was found to be the most uniform and showed good EC performance. These results bode well for further work on CNC-EC composites for specific applications, especially when used on flexible substrates. © The Authors. Published by SPIE under a Creative Commons Attribution 3.0 Unported License. Distribution or reproduction of this work in whole or in part requires full attribution of the original publication, including its DOI. [DOI: 10.1117/1.OE.55.12.127102]

Keywords: tungsten oxide; cellulose nanocrystals; nanocomposites; electrochromic properties.

Paper 161442 received Sep. 15, 2016; accepted for publication Nov. 16, 2016; published online Dec. 8, 2016.

## 1 Introduction

Among transition metal oxides, tungsten oxide (WO<sub>3</sub>) has prompted numerous investigations due to its outstanding electro-<sup>1</sup> and photochromic<sup>2</sup> properties.

Thin tungsten oxide films are suitable for energy-efficient windows, antiglare automobile rear-view mirrors, hydrogen sensors, flat panel displays, and so on.<sup>3</sup>

Although tungsten oxide films can be prepared by various methods, including vacuum evaporation,<sup>4,5</sup> anodic oxidation,<sup>6</sup> spray pyrolysis,<sup>7</sup> sputtering,<sup>8–13</sup> laser ablation,<sup>14</sup> pulsed laser deposition,<sup>15</sup> and vacuum filtration and transfer,<sup>16</sup> the sol–gel technique gained attention due to its simplicity and versatility. Moreover, this method is easy to scale up, and it allows for a precise control of the reactants' concentration. Based on the results of the sol–gel methods, a good understanding exists of the effect of the preparation method and film microstructure on the electrochromic (EC) behavior of the WO<sub>3</sub> films, in particular the kinetics and efficiency of the coloration and the EC cycling stability.<sup>17–19</sup>

In a sol–gel method, the tungsten oxide network is obtained via inorganic polymerization reactions (gelation), starting from molecular precursors such as salts or alcoxides in solution. Gelation takes place upon hydrolysis and condensation of precursors in the presence of water. One of the more commonly utilized sol–gel methods is based on the reaction of the metallic tungsten with hydrogen peroxide that results in the formation of stable solutions of peroxopolytungstic acid, which contains the (W<sub>2</sub>O<sub>11</sub>)<sup>2-</sup> anion.<sup>20–23</sup> By using a dip-coating deposition technique and suitable annealing temperatures, our group and others have prepared nanostructured thin films of tungsten oxide and its gold-doped composites that have very good EC properties.

Cellulose, on the other hand, is a key component in developing and producing new renewable bio-based products on an industrial scale with very few or no nonrenewable sources, as necessary in a circular bioeconomy.

Every monomer of glucose, a monosaccharide, is synthesized in specific enzymatic terminal complexes (TC) in the membrane of the living cells of origin. After synthesis, every second monomer is rotated 180 deg and covalently linked to the adjacent one into a repeating unit, a disaccharide also called cellobiose. These dimers covalently link to one another into linear and stiff molecular chains or polysaccharide<sup>24–26</sup> with an average number or degree of polymerization in the range of 200 to 15,000, depending on their source.<sup>27</sup> Owing to the three hydroxyl groups of each glucose monomer of the chain, strong hydrogen bonds are established between neighboring chains, which are thus assembled into elementary fibrils or microfibrils of lateral dimension between 1.5 and 3.5 nm. Driven by van der Waals forces and due to their nanoscopic sizes and high surface energy, these elementary fibrils further pack together into larger microfibrils of diameter between 10 and 30 nm and finally into microfibrillar bands of about 100 nm diameter.<sup>24</sup>

After their synthesis, glucose monomers can be perfectly linked to one another, forming well-ordered or crystalline regions, or they can be linked with defects or dislocations, building amorphous regions if the TCs encounter adverse conditions. The crystalline regions further consolidate with a complex network of intra- and intermolecular hydrogen-bonds into needle-like shapes known as cellulose nanocrystals (CNCs) and revealed by, for example, TEM images.<sup>25,26</sup>

CNCs can be extracted from cellulose fibers by acid hydrolysis of the amorphous region of the microfibrils. Different acids have been used, with different effects.<sup>28</sup>

This work was initially motivated by the excellent properties of the CNCs, especially the mechanical strength that they may impart to different composite materials [CNC has a high

\*Address all correspondence to: Vo-Van Truong, E-mail: [truong.vo-van@concordia.ca](mailto:truong.vo-van@concordia.ca)

tensile strength (7.5 to 7.7 GPa), elastic modulus (110 to 220 and 10 to 50 GPa in axial direction and transverse direction, respectively)].<sup>29,30</sup>

The theoretical value of Young's modulus along the chain axis for perfect native CNCs is estimated to be 167.5 GPa, which is even stronger than steel and similarly strong as Kevlar,<sup>31</sup> while the elastic modulus of native CNCs extracted from cotton and tunicate reach up to 105 and 143 GPa, respectively.<sup>32,33</sup> Combining CNCs and tungsten oxide may result in a nanocomposite having good EC properties and enhanced mechanical ones.

Numerous composite materials based on CNCs and organic polymers have been reported in the literature.<sup>34,35</sup> For instance, the Yamazaki group<sup>36</sup> used tungsten methylcellulose composite films as photochromic material.

WO<sub>3</sub>-CNC composites are, thus, especially worth being investigated to find out how the presence of CNC would affect the EC properties and their stability with cycling; as such, a composite can hold the promise for a "smart" EC reinforced material.

In this work, as far as we know, we report an original study on the structure, morphology, and EC properties of CNC–tungsten trioxide composites prepared by a dip-coating method. To this purpose, CNCs were mechanically mixed with the tungsten oxide precursor solution, and thin films of the composite were subsequently deposited on indium-tin-oxide (ITO)-coated substrates.

Owing to the existence of six superficial OH groups of each CNC repeat unit which can establish H-bonds with the oxygen atoms of the WO<sub>3</sub>, we expect a good compatibility between the WO<sub>3</sub> matrix and its CNC fillers. Therefore, it is estimated that the risk of expulsion of the CNCs out of the matrix is small. At the same time, since the H-bonds are weak, the CNCs may retain their mobility within the matrix solution; thus, they can be dispersed relatively uniformly throughout the matrix volume. Thus CNCs can also establish H-bonds between themselves, building a network, as suggested in Fig. 1.

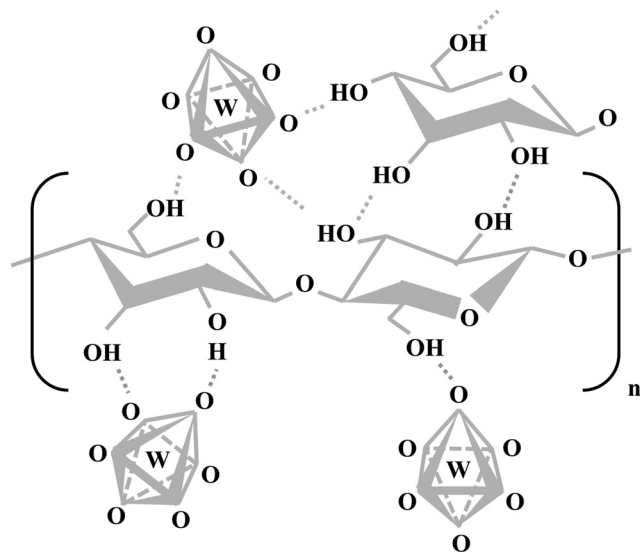


**Fig. 1** Schematic of the possible hydrogen bonds formed between the CNCs and WO<sub>3</sub> molecules and among the CNCs.

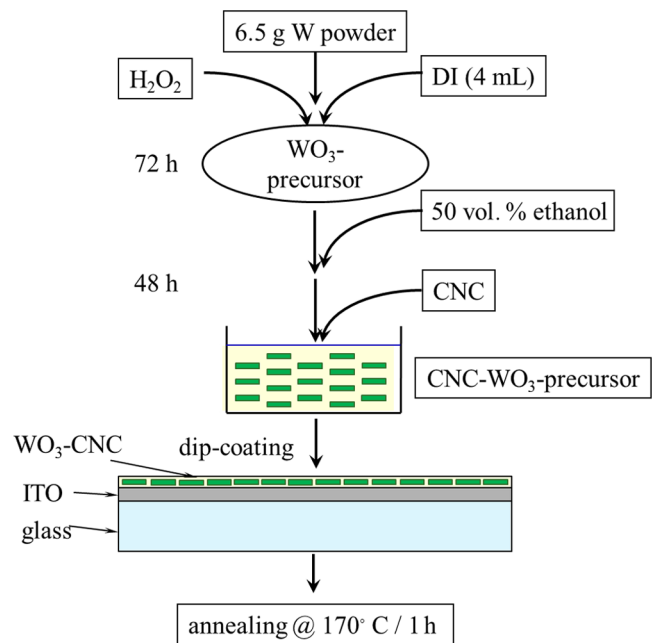


**Fig. 2** Flowchart showing the fabrication of tungsten oxide-CNC nanocomposite film.

## 2 Experimental

Tungsten oxide was prepared via a sol-gel method by using the peroxopolytungstic acid precursor solution. The precursor was synthesized via the reaction of metallic tungsten powder (6.5 g) with 40 mL of concentrated (30%) hydrogen peroxide solution diluted with 4-mL deionized water (DI). The reaction is strongly exothermic, and, in the beginning, it has to be cooled in a water bath to allow the reaction to take place at a temperature of around 5°C. After the reaction is finished, the solution is diluted by adding an equal volume of ethanol [50% (v/v) based on the precursor solution] as indicated in Fig. 2. To ensure that the excess hydrogen peroxide is decomposed, the solution is kept for at least 48 h, until it turns a light yellow color, transparent, and with no visible oxygen bubbles, before using it.

CNCs extracted from wood pulp in an aqueous solution with 11.5% weight concentration was provided by the process development center of the University of Maine. It was then added to the peroxipolytungstic acid precursor solution and thoroughly mixed in a blender at room temperature. Prior to film deposition, the ITO-coated glass of 1 mm thickness, purchased from Colorado concept coatings LLC, was cut in pieces of 20 × 40 mm, cleaned by sonication in acetone, isopropyl alcohol and DI for 20 min each, and dried at 110°C for 1 h. To deposit the films, the ITO-coated glass slides were dipped into the well-stirred solution of the WO<sub>3</sub> precursor mixed with CNC, using a PTL-MM02 dip-coater machine from MTI Corporation, with down- and upward traveling speeds of 45 and 60 mm/s, respectively, and a dwell time of 2 min. The structure and morphology of the films were studied using x-ray diffraction (XRD), field emission-scanning electron microscopy, and atomic force microscopy (AFM). The EC performance was analyzed by cyclic voltammetry using a CH Instruments electrochemical analyzer, an Ocean Optics halogen light source, and an UV-vis-NIR spectrometer. A three-electrode cell was used, where the WO<sub>3</sub>-CNC film on the ITO/glass substrate is the

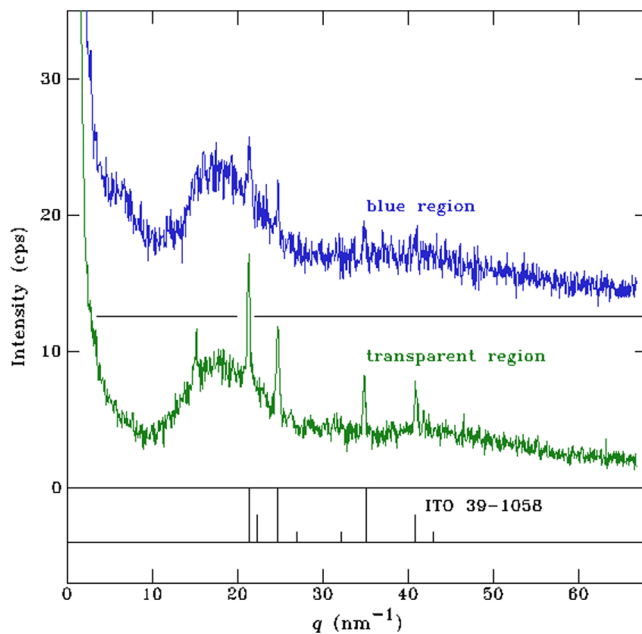


**Fig. 3** XRD patterns of  $\text{WO}_3$ -CNC composite films deposited on ITO-coated glass. The blue curve, corresponding to the central region of the sample, was in contact with the electrolyte and contains intercalated lithium ions. The green curve corresponds to the pristine material.

working electrode, Ag/AgCl the reference electrode, and Pt the counter electrode. The electrolyte used in the experiment was a 1M solution of lithium perchlorate ( $\text{LiClO}_4$ ) in propylene carbonate ( $\text{C}_4\text{H}_6\text{O}_3$ ).

XRD measurements of the films on glass were carried out in reflection mode with a custom-built theta-theta diffractometer equipped with graphite monochromator and analyzer crystals.  $\text{CuK}\alpha$  radiation was used, and the data are shown as a function of the modulus of the scattering vector  $q = 4\pi\lambda^{-1} \sin(\theta)$ , where  $2\theta$  is the scattering angle.

### 3 Results and Discussion

Experiments were conducted to establish the maximum content of CNCs possible to be integrated in an EC composite

without adverse effect on uniformity and EC performance. To this end, a range of concentrations between 5% and 40% were tested, and a concentration of 10% was found to be optimal. Films of higher concentration were nonuniform, had smaller transmittance modulation, and a shorter cycling life. Multilayer films of the same composition as well as alternating  $\text{WO}_3$  and 10%  $\text{WO}_3$ -CNC were also tested, but a single layer of 10% CNC in  $\text{WO}_3$  showed the best results.

The remainder of the article presents results obtained with films of this composition.

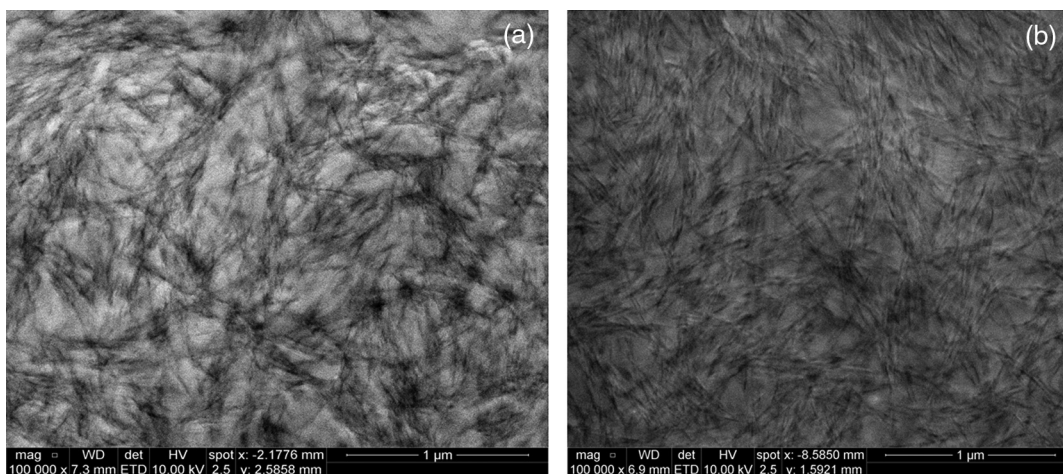
#### 3.1 Structure and Morphology of the $\text{WO}_3$ -CNC Composite

Figure 3 shows the XRD patterns of  $\text{WO}_3$ -CNC composite films. The two regions of the film are shown: the central region that was in contact with the electrolyte during cycling (the “blue region”) and the outer colorless region.

The crystalline peaks seen in x-ray scattering data correspond to ITO. The vertical lines indicate reference patterns from the JCPDS database entry 39-1058. The intensity of ITO peaks is significantly lower for the region that was in contact with the electrolyte, and no additional peaks were observed. This suggests that the plated film is amorphous in nature. A broad feature from about 2 to 8  $\text{nm}^{-1}$  may correspond to the heterogeneities at length scales of about 3 to 0.75 nm. This length scale correlates with the diameter of the needle-like structures in the SEM and AFM micrographs.

It is noticed that after cycling, the structures of the composite films are changed. This is probably due to the ion–film interaction during the coloration and bleaching cycles. SEM image of the central area of the film, colored after  $\text{Li}^+$  intercalation, is shown in Fig. 4(a), while the pristine zone of the same sample is shown in Fig. 4(b).

The CNC network that contains a fairly high density of CNCs can be seen in both Figs. 4(a) and 4(b). However, the image of the  $\text{Li}^+$ -intercalated area (blue) shows a higher porosity, where the CNCs appear to be sparser compared with the “outside” area. Because of the high density of the CNC network, it is difficult to extract information regarding the size of the crystals.



**Fig. 4** SEM images of the  $\text{WO}_3$ -CNC composite: (a) the zone affected by electrolyte, containing the intercalated  $\text{Li}^+$  (the blue region of the sample) and (b) the pristine zone of the sample (outside of the area of contact with the electrolyte).

The AFM images of Figs. 5(a) and 5(b) point toward the same scenario. Indeed, the image of the central part of the sample containing the intercalated  $\text{Li}^+$  ions [Fig. 5(a)] shows a less dense network of CNC compared to the one of the peripheral part of the sample.

The average roughness ( $R_a$ ) of the pristine sample (Fig. 6) and  $\text{Li}^+$  intercalated regions are 9.57 and 11.4 nm, respectively. Root mean square roughness is also similar, 12.2 and 14.5 nm for pristine and  $\text{Li}^+$  intercalated samples, respectively. The CNCs widths in AFM images appear somewhat larger, possibly due to the well-known broadening effect of the AFM tips, which are of sizes comparable to the widths of the CNCs.<sup>19</sup>

Although the CNCs seem to connect pairwise, the CNCs appear evenly dispersed and randomly oriented. Such a distribution of the CNCs would endow the composite film with potentially enhanced mechanical properties. The lack of large agglomerations of CNCs also confirms that CNCs extracted by acid hydrolysis remain sufficiently charged negatively to enable them to repel each other strongly enough and stay separated during the subsequent mixing and coating steps. For this reason, the use of surfactants was not considered necessary.

Since the AFM topographs of the nanocomposite were not clear enough to allow the estimation of the CNCs aspect ratio, a solution of very low CNC concentration in water (0.03 wt. %) was prepared and deposited on a mica substrate. The average aspect ratio of the CNCs was estimated as 20 from the topograph in Fig. 7.

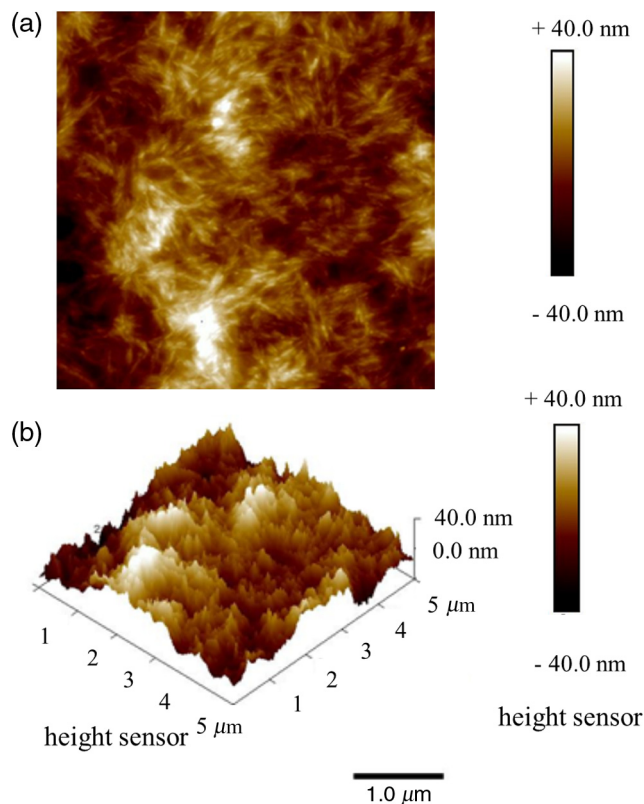


**Fig. 5** AFM images of the  $\text{WO}_3$ -CNC composite: (a) the pristine region of the sample (not in contact with the electrolyte) and (b) 3-D image of the same sample.

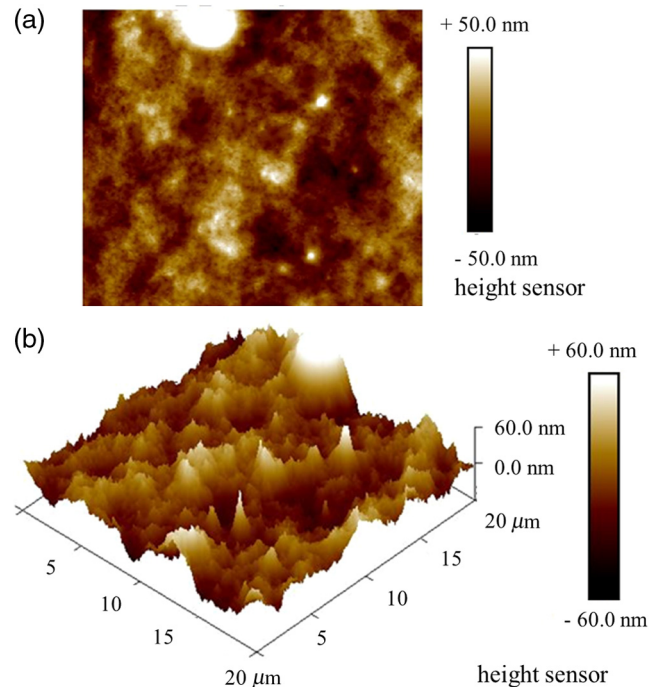


**Fig. 6** (a) AFM image of the central part of the sample containing the intercalated  $\text{Li}^+$  (blue) and (b) the corresponding 3-D image.

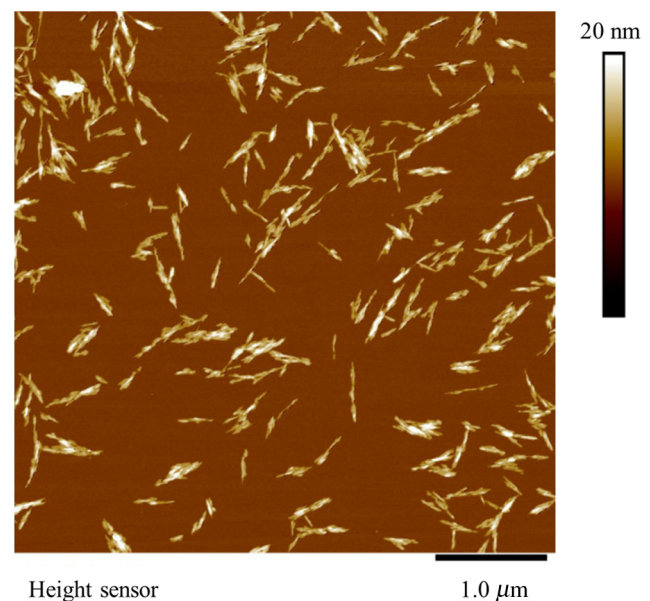


**Fig. 7** AFM topograph of the CNCs deposited from water solution on a freshly peeled mica sheet.

### 3.2 Electrochromic Properties of the $\text{WO}_3$ -CNC Composite

Figure 8 shows the voltammograms of the nanocomposite film cycled from one to 300 times, at a scanning rate of 0.03 V/s.

The voltammograms of the cycled films show a well-defined peak of reduction around 0.210 V while the corresponding oxidation peak was not clearly seen.

As seen in Fig. 9, the optical modulation of the CV experiments (Fig. 8) increased gradually and reached a stable value

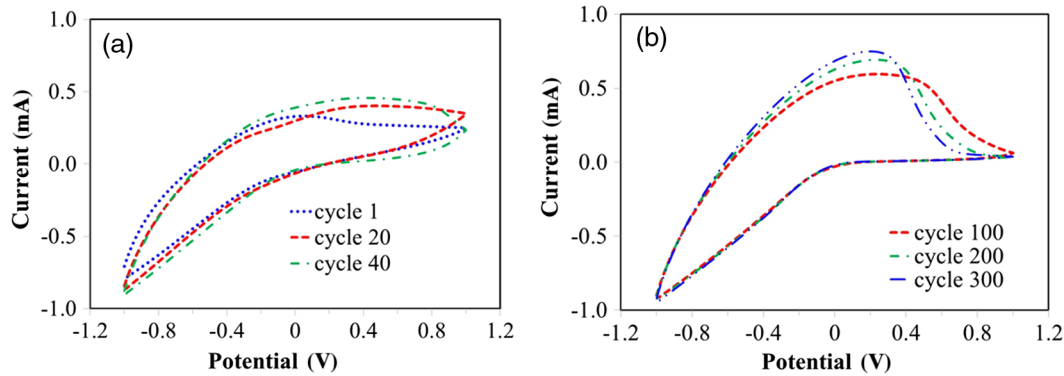


**Fig. 8** Voltammograms in (a) the interval of unsteady transmittance of the first 40 cycles (as shown in Fig. 9) and (b) the interval of stabilized transmittance of the last 200 cycles.

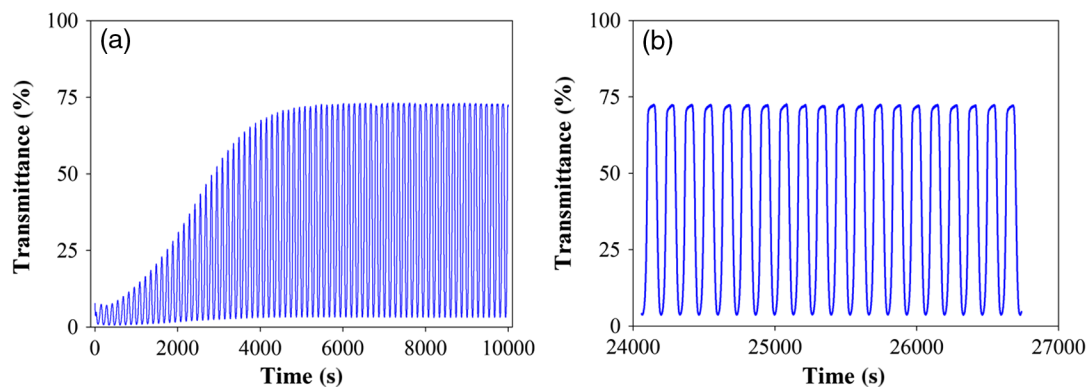


**Fig. 9** Cycle reversibility and transmittance modulation at 600 nm and 0.03 V/s scan rate during (a) the first 75 EC cycles and (b) the last 20 out of the total of 300 cycles carried out.

only after  $\sim 75$  cycles. After that, it remained stable during the whole cycling time. The maximum value found for the nanocomposite films is around 70%, as shown in Table 1.

Figure 10 and Table 1 show the optical modulation in the visible and near-infrared regions.

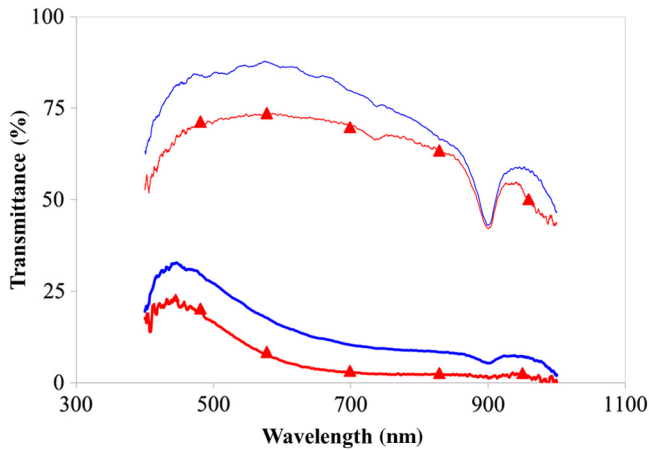
Transmittance spectra at 300 cycles of the  $\text{WO}_3$ -CNC composite and  $\text{WO}_3$  films present modulations of  $\Delta T_{300} = 73.4\%$  and  $\Delta T_{300} = 74.6\%$ , respectively. These values are quite similar, but the transmittance curves for both the bleached and colored states of the nanocomposite film are shifted downward by about 12%, compared to the same curves of the  $\text{WO}_3$  film. These observations show that the CNCs do not alter the transmission modulation of the  $\text{WO}_3$  film but only lower the transmission of light by an additional absorbance (possibly due to a difference in film thickness) and by scattering.

Figure 10 shows that the optical modulation of the nanocomposite films is good over the whole visible and near-IR region of the spectrum. It seems that the modulation is slightly higher in the visible compared with the near-IR for both films.

Table 1 shows the effect of the annealing conditions on the optical modulation of the film. The results indicate that the highest modulations (73% to 75%) correspond to films annealed at 170°C for the duration of 1 h. Increasing the temperature to 180°C or 190°C leads to a slightly lower modulation. The heating temperature is limited by the

**Table 1** Optical modulation under varying annealing conditions.

Annealing conditions			
Temperature (°C)	Duration (min)	$\Delta T_{\max}$ (%)	Comments
170	60	73.6	
170	60	76.3	
170	60	75.7	
180	20	60.0	
180	30	68.0	
190	15	56.5	
200	10	43.3	Light brown color
200	10	52.0	Light brown color
200	15	76.5	Light brown color
200	15	69.5	Light brown color
200	60	59.0	Brown color
200	60	66.0	Brown color



**Fig. 10** Transmittance spectra of the nanocomposite and reference ( $\text{WO}_3$ ) films are shown as red lines marked with triangles and unmarked blue lines, respectively. The thin and thick line curves represent the bleached and colored states of the films, respectively.

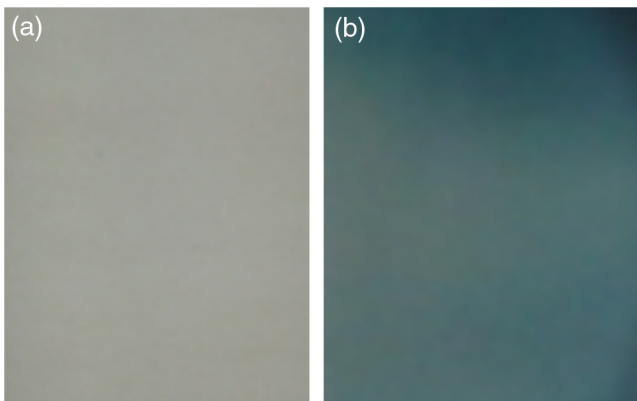


**Fig. 11** The two states of the film: (a) oxidized and (b) reduced.

thermal stability of the CNCs. While the optical modulation appears to be good at even  $200^\circ\text{C}$ , the films become light brown because of a beginning process of decomposition. In addition, after 50 to 100 cycles on this particular film the nanocomposite begins to lose its EC properties.

The colors of the oxidized (bleached)/reduced (colored) states of the film are shown as the parts (a) and (b) of Fig. 11, respectively, corresponding to the switched “off” or “on” of the voltage.

To characterize the speed of color change of the film, response times were defined with respect to the 90% of the maximum transmittance, denoted by “ $T_{90}$ ,” and the minimum transmittance  $T_{\min}$  in a cycle. Thus, the bleaching response time was defined as the time required by the film to reach  $T_{90}$  starting from  $T_{\min}$ , and the coloration time was defined as the time required to reach  $T_{\min}$  starting from  $T_{90}$ . The response times of the  $\text{WO}_3$ -CNC composite were in the range of 10 to 20 s for both bleaching and coloring, which is longer than the response time of the  $\text{WO}_3$  alone (4 to 7 s), prepared under the same conditions.

#### 4 Conclusions

We were able to deposit uniform composite films of tungsten oxide–CNC by dip-coating method. The optical and EC properties of these films were analyzed and compared

with the properties of  $\text{WO}_3$  films. The EC properties of the  $\text{WO}_3$ -CNC composites were found to be good and comparable to the corresponding properties of the sol–gel prepared  $\text{WO}_3$ . The EC characteristics of the nanocomposite films were also very stable with respect to cycling. Results found in this work can be further developed to establish the optimal conditions for fabricating  $\text{WO}_3$ -CNC composite films that can be used in various EC applications. In particular, this dipping method can be readily extended to flexible substrates such as ITO-coated polyethylene terephthalate.

For analyzing the shift in transmittance for CNC- $\text{WO}_3$  compared with  $\text{WO}_3$  alone, as future work, an integrating sphere-based spectrometer could be used to measure the optical properties.

#### Acknowledgments

The authors wish to gratefully acknowledge financial support from the Natural Sciences and Engineering Research Council of Canada, which made this work possible.

#### References

1. P. Yang, P. Sun, and W. Mai, “Electrochromic energy storage devices,” *Mater. Today* **19**(7), 394–402 (2016).
2. T. He and J. Yao, “Photochromism in composite and hybrid materials based on transition-metal oxides and polyoxometalates,” *Prog. Mater. Sci.* **51**, 810–879 (2006)
3. C. G. Granqvist, “Oxide-based chromogenic coatings and devices for energy efficient fenestration: brief survey and update on thermochromics and electrochromics,” *J. Vac. Sci. Technol. B* **32**, 060801 (2014)
4. O. Bohnke et al., “In situ optical and electrochemical characterization of electrochromic phenomena into tungsten trioxide thin films,” *Sol. Energy Mater. Sol. Cells* **25**, 361–374, 1992.
5. P. V. Ashrit, G. Bader, and V-V. Truong, “Electrochromic properties of nanocrystalline tungsten oxides thin films,” *Thin Solid Films* **320**, 324–328 (1998).
6. A. Mozalev et al., “Nanostructured columnlike tungsten oxide film by anodizing Al/W/Ti layers on Si,” *Chem. Mater.* **20**, 6482–6493 (2008).
7. C.-Y. Kim et al., “Tungsten oxide film synthesis by spray pyrolysis of peroxotungstic acid and its electrochromic characterization,” *J. Ceram. Process. Res.* **10**(6), 851–854 (2009).
8. B. W. Faughnan, R. S. Crandall, and P. M. Heyman, “Electrochromism in  $\text{WO}_3$  amorphous films,” *RCA Rev.* **36**, 177–197 (1975).
9. H. Sadiki et al., “Properties and electrochromic performances of reactively sputtered tungsten oxide films with water as reactive gas,” *Surf. Coat. Technol.* **200**, 232–235 (2005).
10. H.-C. Chen et al., “Electrochromic and optical properties of tungsten oxide films deposited with DC sputtering by introducing hydrogen,” *Appl. Opt.* **53**, A321–A329 (2014).
11. A. Subrahmanyam and A. Karupphasamy, “Optical and electrochromic properties of oxygen sputtered tungsten oxide ( $\text{WO}_3$ ) thin films,” *Sol. Energy Mater. Sol. Cells* **91**, 266–274, (2007).
12. M. H. Kim et al., “Electrochromic properties of tungsten oxide films prepared by reactive sputtering,” *Jpn. J. Appl. Phys.* **52**, 05EC03 (2013).
13. A. K. Chawla et al., “Effect of sputtering gas on structural and optical properties of nanocrystalline tungsten oxide films,” *Thin Solid Films* **517**, 1042–1046 (2008).
14. A. Rougier, “Characterization of pulsed laser deposited  $\text{WO}_3$  thin films for electrochromic devices,” *Appl. Surf. Sci.* **153**, 1–9 (1999).
15. R. Ghosh, M. Baker, and R. Lopez, “Optical properties and aging of gasochromic  $\text{WO}_3$ ,” *Thin Solid Films* **518**, 2247–2249 (2010).
16. Y. Golestani et al., “Microstructure and electrochromic properties of nanostructured tungsten oxide thin films prepared by the vacuum filtration and transfer method,” *J. Electrochem. Soc.* **161**(14), H909–H916 (2014).
17. M. Deepa et al., “A case study of optical properties and structure of sol-gel derived nanocrystalline electrochromic  $\text{WO}_3$  films,” *J. Phys. D Appl. Phys.* **39**, 1885–1893 (2006)
18. B. Zhao et al., “Efficient electrochromic device based on sol–gel prepared  $\text{WO}_3$  films,” *Ionics* **21**, 2879–2887 (2015).
19. S. Badilescu and P. V. Ashrit, “Study of sol–gel prepared nanostructured  $\text{WO}_3$  thin films and composites for electrochromic applications,” *Solid State Ionics* **158**, 187–197 (2003).
20. M. Alsawafta et al., “Improved electrochromic properties of vanadium pentoxide nanorods prepared by thermal treatment of sol-gel dip-coated thin films,” *J. Electrochem. Soc.* **162**(7) H466–H472 (2015).

21. Y. Golestani et al., “Microstructure and electrochromic properties of nanostructured tungsten oxide thin films prepared by the vacuum filtration and transfer method,” *J. Electrochem. Soc.* **161**(14) H909–H916 (2014).
22. A. Almoabadi et al., “Subzero temperature dip-coating of sol-gel vanadium pentoxide: effect of the deposition temperature on the film structure, morphology, and electrochromic properties,” *J. Nanomater.* **2016**, 1–10 (2016).
23. M. Alsawafra et al., “Electrochromic properties of sol-gel synthesized macroporous tungsten oxide films doped with gold nanoparticles,” *J. Electrochem. Soc.* **161**(5) H276–H283 (2014).
24. D. Klemm, “Cellulose: fascinating biopolymer and sustainable raw material,” *Angew. Chem. Int. Ed.* **44**, 3358–3393 (2005).
25. Y. Habibi and A. Dufresne, “Nanocrystals from natural polysaccharides,” in *Handbook of Nanophysics*, K. D. Sattler, Ed., CRC Press, Taylor & Francis (2008).
26. P. Zugenmeier, “Crystalline cellulose and derivatives—characterization and structures,” in *Springer Series in Wood Science*, Springer-Verlag, Berlin Heidelberg (2008).
27. J. Yang et al., “Synthesis and characterization of mechanically flexible and tough cellulose nanocrystals–polyacrylamide nanocomposite hydrogel,” *Cellulose* **20**, 227–237. (2013).
28. G. Siqueira et al., “Cellulosic bionanocomposites: a review of preparation, properties and applications,” *Polymers* **2**, 728–765 (2010).
29. B. Peng et al., “Chemistry and applications of nanocrystalline cellulose and its derivatives: a nanotechnology perspective,” *Can. J. Chem. Eng.* **89**, 1191–1206 (2011).
30. K. Tashiro and M. Kobayashi, “Theoretical evaluation of three-dimensional elastic-constants of native and regenerated celluloses: role of hydrogen-bonds,” *Polymer* **32**(8), 1516–1526 (1991).
31. R. Rusli and S. Eichhorn, “Determination of the stiffness of cellulose nanowhiskers and the fiber-matrix interface in a nanocomposite using Raman spectroscopy,” *Appl. Phys. Lett.* **93**(3), 033111 (2008).
32. A. Sturcova, G. Davies, and S. Eichhorn, “Elastic modulus and stress-transfer properties of tunicate cellulose whiskers,” *Biomacromolecules* **6**(6), 1055–1061 (2005).
33. V. Khoshkava and M. Kamal, “Effect of cellulose nanocrystals (CNC) particle morphology on dispersion and rheological and mechanical properties of polypropylene/CNC nanocomposites,” *ACS Appl. Mater. Interfaces* **6**, 8146–8157 (2014).
34. M. Tatsumi, Y. Teramoto, and Y. Nishio, “Polymer composites reinforced by locking-in a liquid-crystalline assembly of cellulose nanocrystallites,” *Biomacromolecules* **13**, 1584–1591 (2012).
35. P. Markiewicz and M. Goh, “Simulation of atomic force microscope tip-sample/sample-tip reconstruction,” *J. Vac. Sci. Technol. B* **13**, 1115 (1995).
36. S. Yamazaki et al., “Photochromic properties of tungsten oxide/methylcellulose composite film containing dispersing agents,” *ACS Appl. Mater. Interfaces* **7**, 26326–26332 (2015).

**Stefan Stoenescu** received his master’s degree from McGill University in 1998 and his doctoral degree from Concordia University in 2013. His research concerned optical properties of nanostructures characterized by mathematical modeling, computer simulations, and validated spectroscopically. As a postdoctoral fellow at the same university, he has expanded his research to nanocomposite films for electrochromic and energy storage applications, some in collaboration with industry.

**Simona Badilescu** is a senior scientist with a background in physical chemistry and a rich experience in teaching and research. She received her PhD from the University of Bucharest (Romania) and specialized in molecular spectroscopy, surface science and, later on, on nanomaterials. She published three books and several chapters, mainly on topics related to nanomaterials. She is author of more than 250 articles and conference papers.

**Tanu Sharma** has been a postdoctoral fellow at Mount Allison University since 2011. She received her doctoral degree from Kurukshetra University, India, in 2008. Currently, she is working on evaluating stress in copper films for the electronics industry. Her general research interests include properties and applications of metal-oxide/composite films, interactions of radiations with polymers, and its influence on optical/structural properties of polymers. She has been a coauthor on more than 25 peer-reviewed publications.

**Ralf Brüning** is a professor of physics at Mount Allison University. He received his doctoral degree from McGill University in 1990. His research interests include x-ray diffraction, properties of glasses (structure and kinetics), metals and metal-oxides, electroless, and galvanic copper plating. He has been coauthor of more than 100 peer-reviewed research articles. He has received several awards from the university for his contributions toward research and teaching.

**Vo-Van Truong** (PhD in physics, U. Toronto, 1976) has contributed principally in the optical properties of thin films and advanced materials, the applications of thin films, and the design of optical metrology instruments. He is author or coauthor of about 150 refereed physics publications and numerous scientific reports. He has also served on several boards of tech-transfer organizations and in senior university management positions. He is presently a professor emeritus at Concordia University.